Supplementary Information for

Dual-Channel Quantum Meta-Hologram for Display

Yubin Fan[1,2,3,#], Hong Liang[4,5,#], Yuhan Wang[6,#], Shufan Chen[1,2,3], Fangxing Lai[6], Mu Ku Chen[1,2,3], Shumin Xiao[6,7,*], Jensen Li[4,5,*] and Din Ping Tsai[1,2,3,*]

[1]Department of Electrical Engineering, City University of Hong Kong, Kowloon, Hong Kong, 999077, P. R. China

[2]Centre for Biosystems, Neuroscience, and Nanotechnology, City University of Hong Kong, Kowloon, Hong Kong, 999077, P. R. China

[3]The State Key Laboratory of Terahertz and Millimeter Waves, City University of Hong Kong, Kowloon, Hong Kong, 999077, P. R. China

[4]Department of Physics, The Hong Kong University of Science and Technology, Clear Water Bay, Kowloon, Hong Kong, 999077, P. R. China

[5]IAS Center for Quantum Technologies, The Hong Kong University of Science and Technology, Clear Water Bay, Hong Kong, 999077, P. R. China

[6]Ministry of Industry and Information Technology Key Lab of Micro-Nano Optoelectronic Information System, Guangdong Provincial Key Laboratory of Semiconductor Optoelectronic Materials and Intelligent Photonic Systems, Harbin Institute of Technology (Shenzhen), Shenzhen, 518055, P. R. China

[7]Pengcheng Laboratory, Shenzhen, 518055, P. R. China

[#]These authors contribute equally to this work

Supplementary Information Note-1: The numerical simulation and fabrication of meta-holograms

1.1 The numerical simulation of meta-holograms

The numerical calculation of the meta-hologram phase unit is designed by COMSOL Multiphysics. We selected the working wavelength as 810 nm according to SPDC process and our pump laser. The unit's height is set as 1 μm, the period as 500 nm and the width (w) and depth (d) range from 100 nm to 450 nm. Later we swept the weight and depth of a unit in COMSOL as 10 nm per step to maintain the phase accuracy of the phase plate. Finally, we extracted the phase and transmission of input linear polarized plane wave in the wavelength domain. The results show in Figure S1(a-b). We directly flip the weight and depth as the unit size is symmetric for both linear polarizations Fig.S1(c-d). Until now, we have got the phase and transmission of the unit cell.

The next step is generating meta-holographic phase mapping. We use the G-S algorithm to generate phase profiles for both polarizations separately, shown in Figure S2. The transmission units under 90% are excluded while mapping to maintain the efficiency of the meta-hologram. As there are two channels needed

in realizing a set of structural units, we select two polarized phases by simply minimizing phase differences, expressed as follows,

$$\mathrm{Min}(\mathrm{Abs}(\exp(iP_H(x,y)) - \exp(iP_{H_0}(x,y))) * \mathrm{Abs}(\exp(iP_V(x,y)) - \exp(iP_{V_0}(x,y))))$$

Where $P_{H(V)}(x,y)$ is the phase library of H(V) polarization extract from the last step, and $P_{H(V)_0}(x,y)$ is the desired phase for H(V) channel.

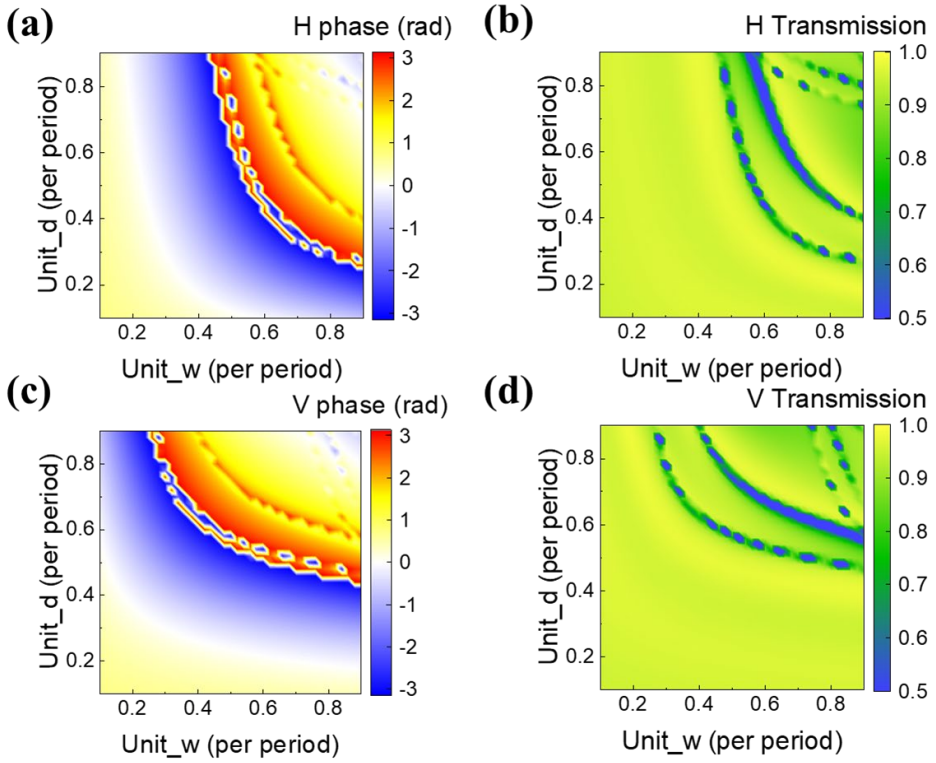

Figure. S1 (a) Unit phase and (b) transmission of H polarization for the unit cell. After flipping the axis, we obtain (c) Unit phase and (d) transmission of V polarization for the unit cell.

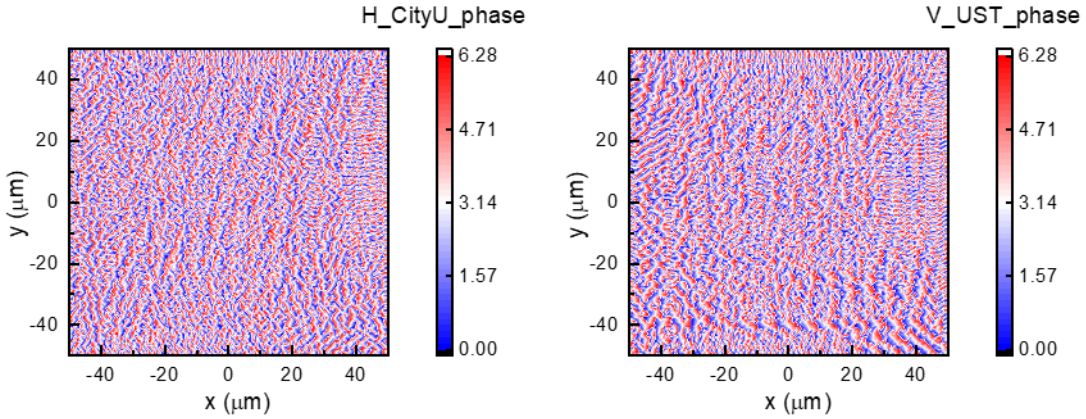

Figure. S2 Phase distribution for meta-hologram (a) H ‘CityU’ and (b) V ‘UST’ polarizations.

1.2 The fabrication of meta-holograms

Based on the numerical calculation and meta-hologram design, the meta-hologram sample is fabricated by the process. The manufacturing process is summarized in Figure S3. First, the 1 μm TiO_2 film, deposited on 13 nm ITO, coated with 200 nm photoresist (PMMA A2)) was patterned by electron beam lithography (Raith Eline 150Plus). After irradiation, the samples were developed in the developer solution (MIBK/IPA with a ratio of 1:3) for 30s. To obtain high selection ratio, Cr film is selected as the etching mask: 30 nm Cr film is deposited, then lift off by remover PG. Finally, the TiO_2 cuboid was formalized by RIE dry etching process (Oxford PlasmaPro 800). The refractive index of TiO_2 is set as 2.178 according to the ellipsometer in Figure S4.

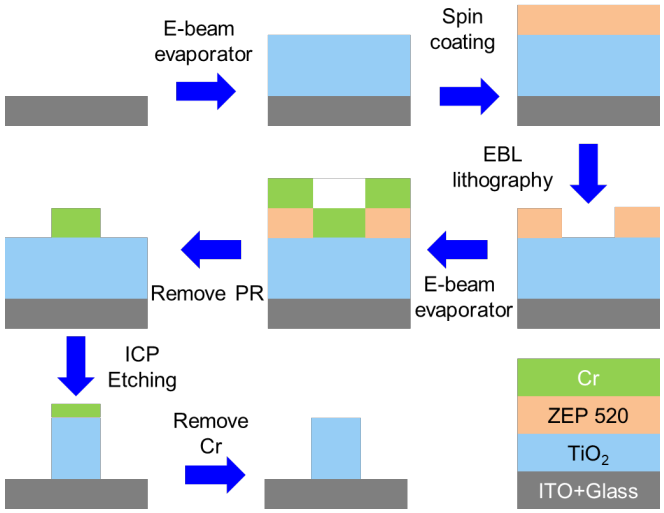

Figure. S3 Fabrication process of meta-hologram

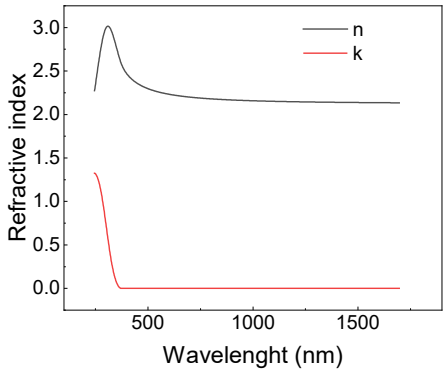

Figure. S4 Refractive index of TiO_2 used in this work

Supplementary Information Note-2: Optical characterization of meta-hologram

2.1 The optical setups for classical source characterization

Figure S5(a) shows the optical setups for classical source characterization. The setup mainly includes a beam reduction part and a pack focal plane (BFP) imaging part. The beam reduction part is composed of a 10 cm tube lens and a 20x objective lens. Before the reduction lens pair, an HWP is used to adjust the polarization illuminated on the sample. The beam reduction part decreases the classical incident linear polarized beam (810 nm from FIU-6, NKT Photonics) to smaller than the metasurface sample size and in a small incident angle.

The correlation between quantum heralding holograms sample and input linear polarizations is demonstrated in Figure S5(b). Specifically, only the corresponding polarization hologram is observable when the input is either V or H polarization. However, if the sample is fed with 45-degree (Diagonal, D) polarization, both holograms become visible.

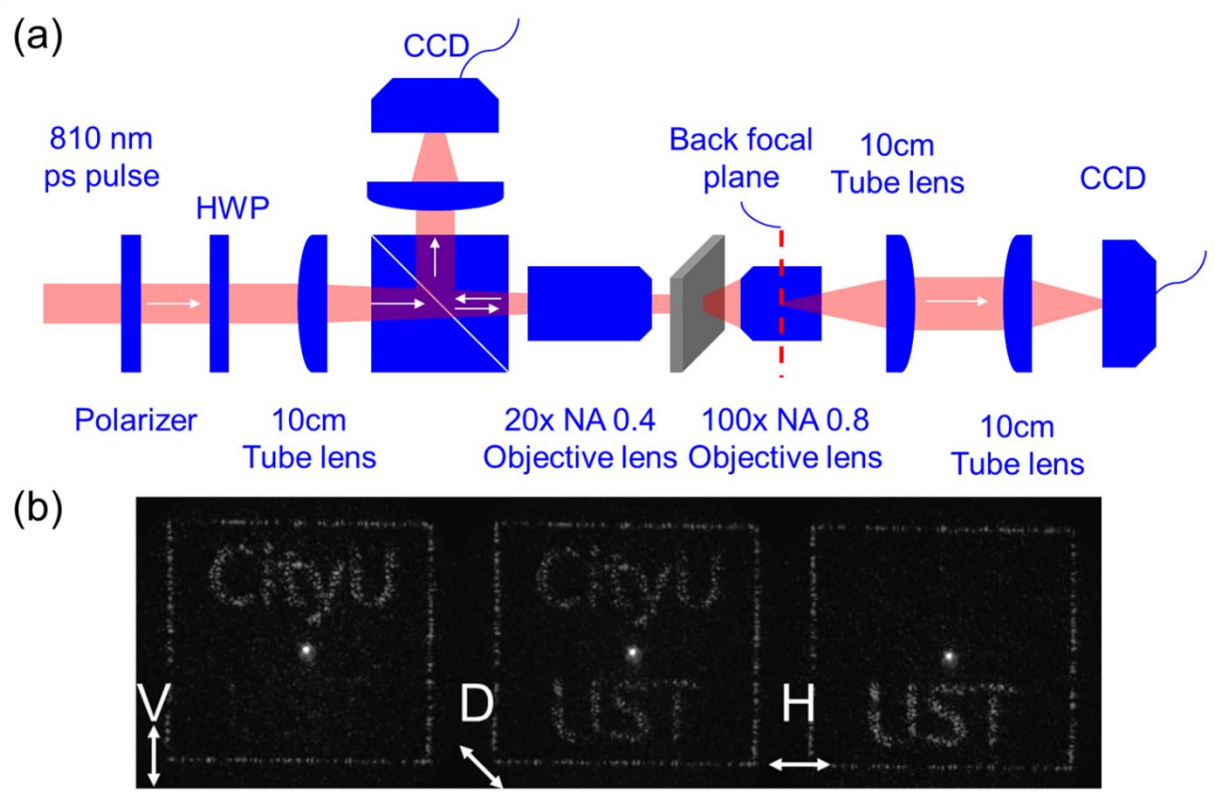

Figure S5 The optical setup and simple placement for classical light source characterization. (a) The optical setup and (b) Relations between quantum heralding holograms sample and input linear polarization.

After interacting with the metasurface, the BFP imaging part collects the signal. A high NA objective lens works as a Fourier transforms lens, changing the phase information in the focusing plane to meta-holographic imaging in BFP. A pair of 10 cm tube lenses transferred the meta-holographic imaging from BFP to the CCD plane. Thus, we can get meta-holographic imaging collected by CCD and shown on computers or screens.

2.2 The optical setups for quantum correlation imaging characterization

After confirming the polarization-dependent holograms by classical light, we now move on to the quantum optical imaging of the metasurface using heralding photons. The optical setup for the classical light source works as a signal arm of the optical setup for quantum correlation imaging, shown in Figure S6. We use a 2-mm-thick type-II BBO and a 200mW 405 nm laser (CrystaLaser DL-405-400) to generate the polarization-entangled photon pairs in a state of $1/\sqrt{2}(|HV\rangle + |VH\rangle)$. The half opening angle of the generated photon pairs is designed to be 3°. The photons are split into the signal arm and heralding arm. To compensate the translational and longitudinal walk-off effects of the photon pairs, there are an HWP at 45° and a BBO with half of the thickness of the main BBO in both arms.

The photons in the heralding arm are detected with polarization selection (horizontal or vertical) using a single photon counting module (SPCM) (Excelitas-SPCM-800-14-FC), and the detection signals are sent to herald signal photons' arrival on the single photon avalanche diode (SPAD) camera. Meanwhile, the signal photons are sent to the imaging setup through a 10-meter-long single-mode fiber. The HWP before the metasurface is used to correct the polarization rotation due to the long fiber so that the input quantum states on the metasurface are $1/\sqrt{2}(|HV\rangle - |VH\rangle)$. The polarization state is checked with a flip mirror to direct the light into fiber coupler 4 and detected with SPCM2 (dashed light path). The SPCM2 is correlated with SPCM1 with a correlator (UQD-Logic-16). We then use a lens (focal length 100 mm) with a 20x objective to focus the signal beam onto the metasurface. The hologram generated from the metasurface is imaged on the SPAD camera (SPAD512S) using a 60x objective along with the two lenses of focal length at 150 mm and 45 mm.

The intensity profile of the holograms in Figure 3(b) is acquired using 6000 frames with the background subtracted. Each frame spans 100 ms with a maximum of 255 photon counts in each pixel. The background is taken with the signal photons and additional noise blocked. The heralding image of the holograms in Figure 3(c,d) are all retrieved using 6000 frames with an external trigger from the detection of the photons in the heralding arm and with background subtracted. Each frame spans 100 ms with a maximum of 255 photon counts in each pixel. Each trigger would turn on the camera for a detection window of 10 ns. With heralding photon counting rate up to 250 kHz, there would be multiple triggers in one frame, and the detection events in each triggered window would accumulate into one frame. The background is measured using the same triggering setting with blocked signal photons.

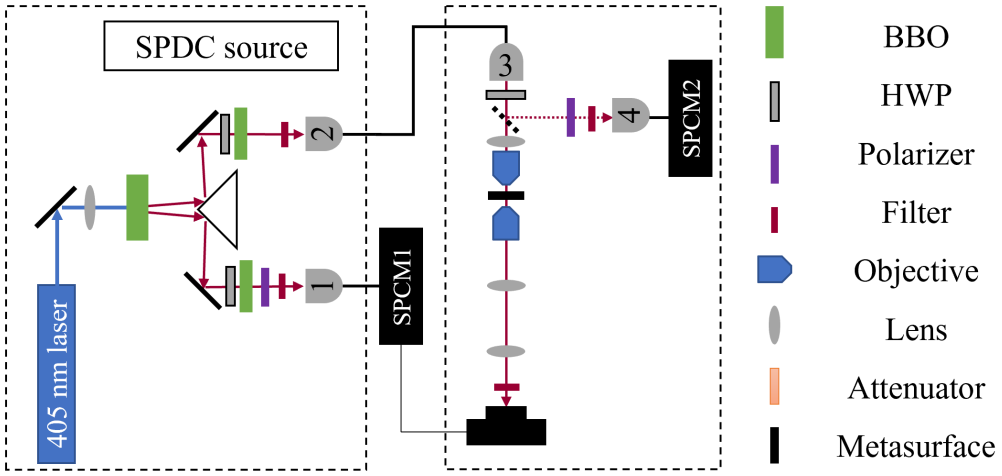

Figure S6 The optical setup for quantum correlation imaging characterization.

2.3 The optical setups for eliminating multiple residual lights display

To further show that the heralding holograms are robust to noise, including multiple reflective light and speckles, based on the optical setup in Figure S6, we add an 810 nm laser acting as noise, as shown in Figure S7. The 810 nm laser is attenuated and combined with the imaging light with a 50:50 beamsplitter. As shown in Figure 4(a), we generate the speckle noise using the beam expander with uncleaned surfaces. To generate the multiple reflection spots shown in Figure 4(c), we use a pair of face-to-face 50:50 beamsplitter with a slightly unparallel surface. Figure 4 (b/d) is acquired in the same condition as Figure 4 (a/c). The procedure to take images in Figure 4 is the same as that in Figure 3. The background is taken with the signal photons, and the additional noise illumination is blocked and gets subtracted.

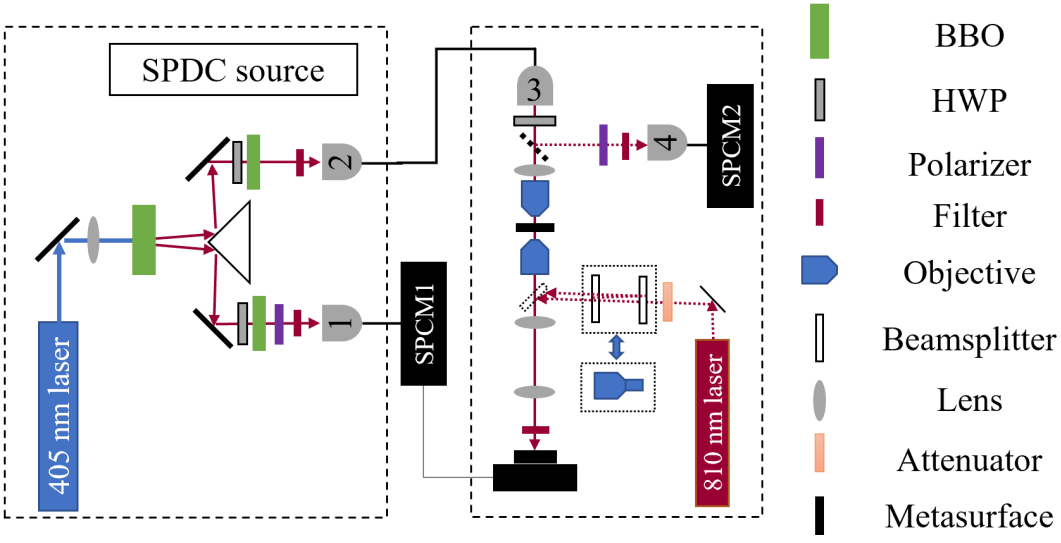

Figure S7 The optical setup for testing noise robustness of the heralding holograms.

Supplementary Information Note-3: Method of quantitative analysis meta-hologram

3.1 The calculation of the Pearson correlation coefficient, the signal-to-noise ratio (SNR)

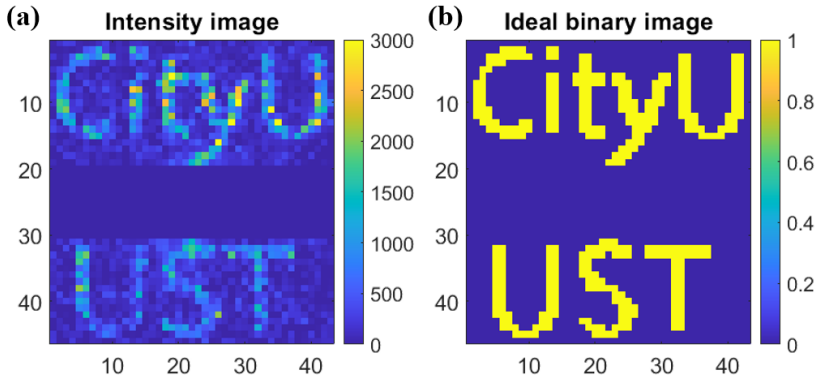

Figure S8 Comparing experimental image with an ideal binary image. (a) Experimental image of the hologram with center residue spot and outer rectangular frame removed. (b) Resized and binarized ideal hologram images with the same size as the experimental ones.

To denote the quality of our imaging system, we use the Pearson correlation coefficient and the signal-to-noise ratio (SNR). The ideal target image is resized and binarized to have the same resolution as the experimental images. Compared with the ideal image, we remove the center residue spot and focus only on the letter part, excluding the outer rectangular frame (Figure S8). The Pearson correlation coefficient is then calculated as

$$r_{mt} = \frac{\sum_i^n (m_i - \bar{m})(t_i - \bar{t})}{\sqrt{\sum_i^n (m_i - \bar{m})^2}\sqrt{\sum_i^n (t_i - \bar{t})^2}},$$

Where $m(t)$ denotes the measured experimental (target ideal) image and i denotes the pixel index ranging from 1 to n. To calculate SNR, we use

$$SNR = 20\log_{10}\left(\frac{\sqrt{\sum t_i^2}}{\sqrt{\sum (m_i/s - t_i)^2}}\right),$$

Where s is the 99.5 percentile of m_i counts and is used to renormalize the experimental image. We avoid directly using the maximum count in the image to alleviate the error due to noisy pixel outliers. We calculate the Pearson correlation coefficients and the SNRs for Figures 3(b-d) and 4(a,b), which are summarized as follows.

Table S1 Pearson correlation coefficient and SNR in figures

Image of hologram	Pearson correlation coefficient	SNR
Figure 3(b)	0.73	3.1
Figure 3(c)	0.80	4.4

Figure 3(d)	0.80	4.4
Figure 4(a)	0.35	1.4
Figure 4(b)	0.62	2.4

3.2 The efficiency of the meta-hologram

In the manuscript, we choose one meta-hologram sample to demonstrate the VR display from three groups of samples. Efficiencies of all these samples are higher than 89%. Here we describe the method we measure the efficiency of the meta-hologram.

We first decrease the incident light intensity to a level that CCD is desaturation because the maximum count of CCD is 255. This action means the maximum of the center spot must low than 255. Then we select the area collecting the outer frame of the meta-hologram as the yellow area and sum all the pixel accounts in the area as the denominator. To calculate hologram efficiency, we exclude the transmitted light spot area counts as shown in Figure S9(a, c) red area and sum the rest of the hologram area as a numerator. Thus, we can get the efficiency of the meta-hologram. The efficiency of characters is calculated as well and can be expressed as: $efficiency = \frac{the\ counts\ of\ the\ hologram\ area\ without\ center\ spot}{the\ counts\ of\ the\ hologram\ area\ with\ center\ spot}$

For example, Fig. S9(b) shows that the efficiency of the H meta-hologram is 93%, and the efficiency of characters 'CityU' is 46%. The efficiencies of all three groups of meta-holograms are measured, shown in Table S2.

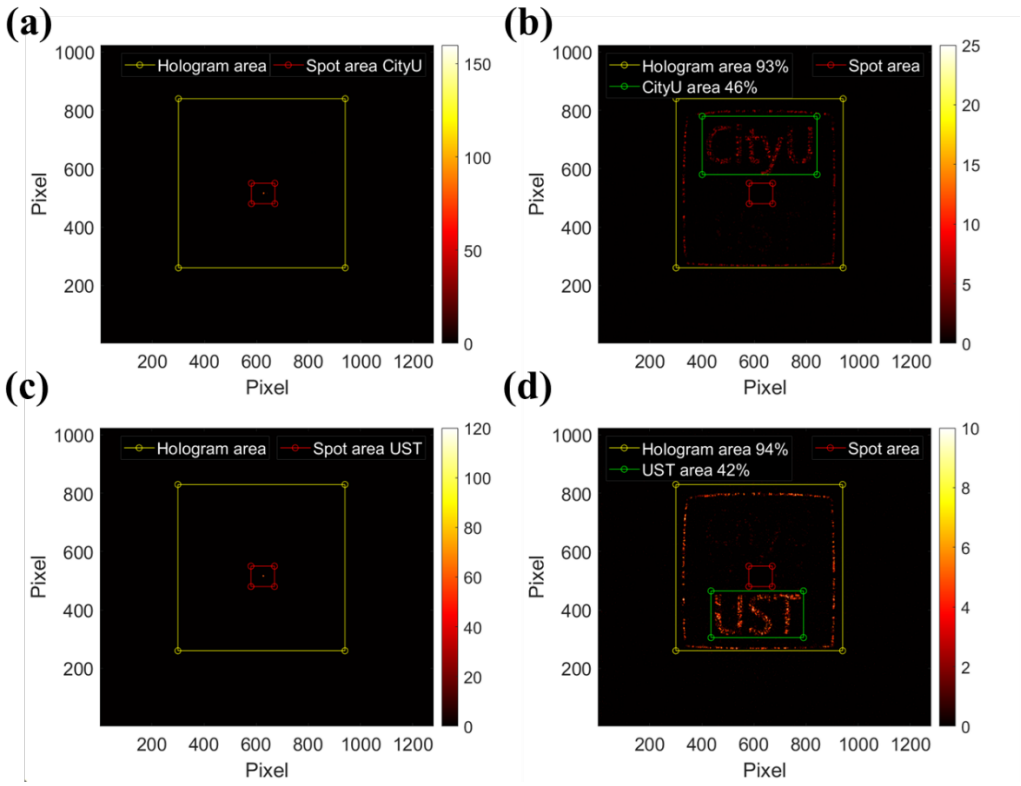

Figure S9 The efficiency calculation of the meta-hologram. H meta-hologram (a) with center spot and (b) without center spot. V meta-hologram (a) with center spot and (b) without center spot

Table-S2: The efficiencies of all three groups of meta-holograms

Sample index		H Hologram efficiency (%)	CityU efficiency (%)	V Hologram efficiency (%)	UST efficiency (%)
Group 1	1	94	47	94	42
	2	94	46	93	42
	3	93	46	93	39
Group 2	1	90	37	92	34
	2	91	38	92	34
	3	90	36	91	34
Group 3	1	91	35	91	42
	2	91	37	91	40
	3	89	38	89	39

3.3 The calculation of the meta-hologram contrast

In the manuscript, we mentioned the contrast of the letters under classical illumination and quantum correlation illumination. Here we describe the method we calculated the contrast of the meta-hologram. We separately select the area of letters, average the pixel counts in the area as $C_{letters}$. The rest area is signed as background, and the pixel counts as C_{bg}. We define the contrast as $10\mathrm{Log}10(\frac{C_{letters}}{C_{bg}})$ dB. Figure S10 shows the average counts of the letters, and the contrast of various letters shows in Table S3. As the speckle positions are random and they may occur or not on the letter positions, the contrast of 'CityU' in Figure 4(a) is a bit larger than that of 'UST'.

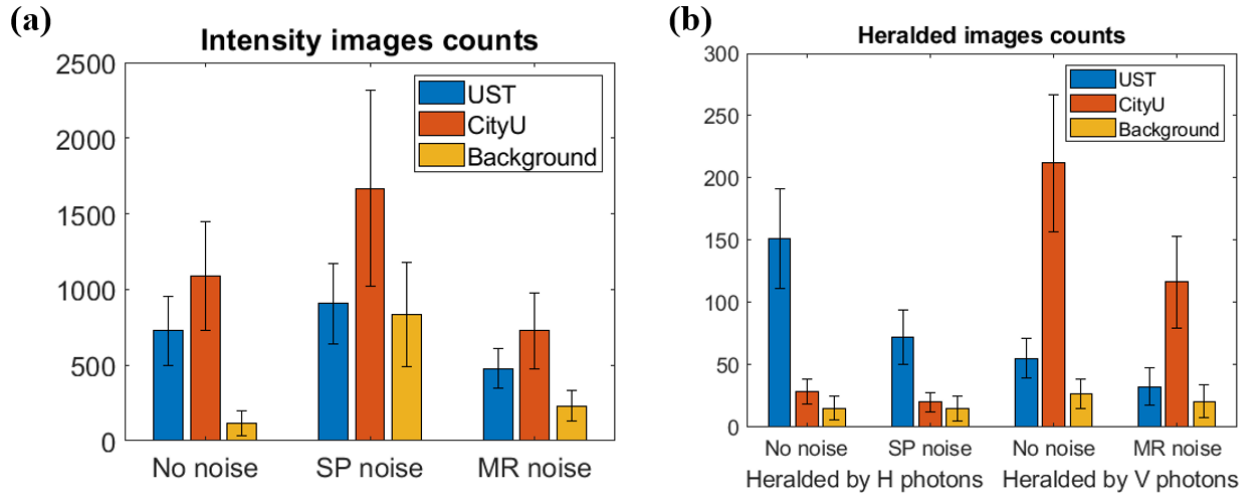

Figure S10 Average intensity counts of letters and backgrounds in figures. The error bar denotes the standard deviation of the counts.

Table-S3: The contrast of all three groups of meta-holograms

Figure index		CityU contrast (dB)	UST contrast (dB)
Figure 3	b	9.8	8.0
	c	9.0	3.2
	d	2.8	10.0
Figure 4	a	3.0	0.36
	b	1.3	6.8

3.4 The discussion of the field of view (FoV) and eyebox

Our FoV and eyebox as shown in Figure S11, are determined by the last lens in the optical path. Taking into account the example of a metasurface hologram with a square side length of 100 μm and an objective magnification of 100x by a $f = 10\ cm$ lens, the equivalent display panel width (w_s) is calculated to be 5 mm with a converging angle $\theta_c = 2\,\mathrm{ArcTan}[diameter\ of\ lens\ /2/f] = 14.5\ Deg$ where the $diameter\ of\ lens = 25.4\ mm$. The FoV is determined by the size of the lens imaging onto the CCD and w_s. Using the optical path described by SI, where the lens has a focal length of $f = 10\ cm$, the FoV can be calculated as

$$FoV = 2\,\mathrm{ArcTan}[diagonal\ size/f] = 8.1\ \mathrm{Deg}$$

The static eyebox, which is the maximum viewing distance that maintains the full FoV, can be defined as

$$w_e = 2d_e\mathrm{Tan}[FOV/2] = 7.1\ mm.$$

Considering a similar platform as Ref.[4] in the manuscript., we replace SLM with the present meta-hologram. As the working wavelength of our meta-hologram is larger than the unit period, the diffraction angle θ_s can not be defined. In this situation, the static eye box is only determined by the diameter of the focal lens.

As a comparison, a related holographic VR device provides a diagonal field of view of 22.8 Deg with a 2.3 mm static eye box as Ref. [4] in the manuscript.

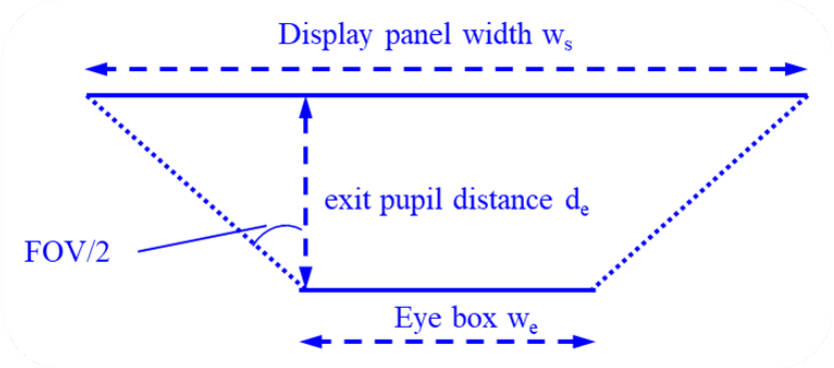

Figure S11 Schematic of FOV and eyebox

Supplementary Information Note-4: Method of quantitative analysis meta-hologram

To collect more photons, we use focused SPDC incident light. The bright central spots are caused by the SPDC beam being incident obliquely or the beam size being slightly larger than the area of the metasurface, resulting in the incident light not being fully modulated. The phase of the structural unit of the metasurface is designed under the condition of normal incidence of plane waves. The oblique incidence will cause the incident light to be unable to be given the designed phase as Figure S12 (a) shows. Taking a cuboid structural unit with a length of 600 nm and a width of 400 nm as an example, moving from normal incidence to 30° incidence, the modulated phase will change from -1.70 rad to 1.52 rad. Oblique incidence on the structural unit will result in undesired phase modulation of the incident light. For example, if 95% of the originally designed phase is modulated and 5% is not modulated, the far-field diffraction pattern is shown in Figure S12 (b), and a bright spot in the center can be observed. We expect that better display quality can be realized by using Kohler illumination to achieve normal incidence and limiting the incident spot size to avoid unmodulated light. The experimental result is shown in Figure S12 (c). Another potential method to avoid the central spot is to implement a holographic display in the near-field (Fresnel) regime. Unlike the current far-field setup where the unmodulated light appears as a bright central spot at the zeroth order, they serve as a uniform background which typically has a negligible effect on visual quality. Taking 95% modulated and 5% unmodulated light as an example, the calculation result is shown in Figure S12 (d).

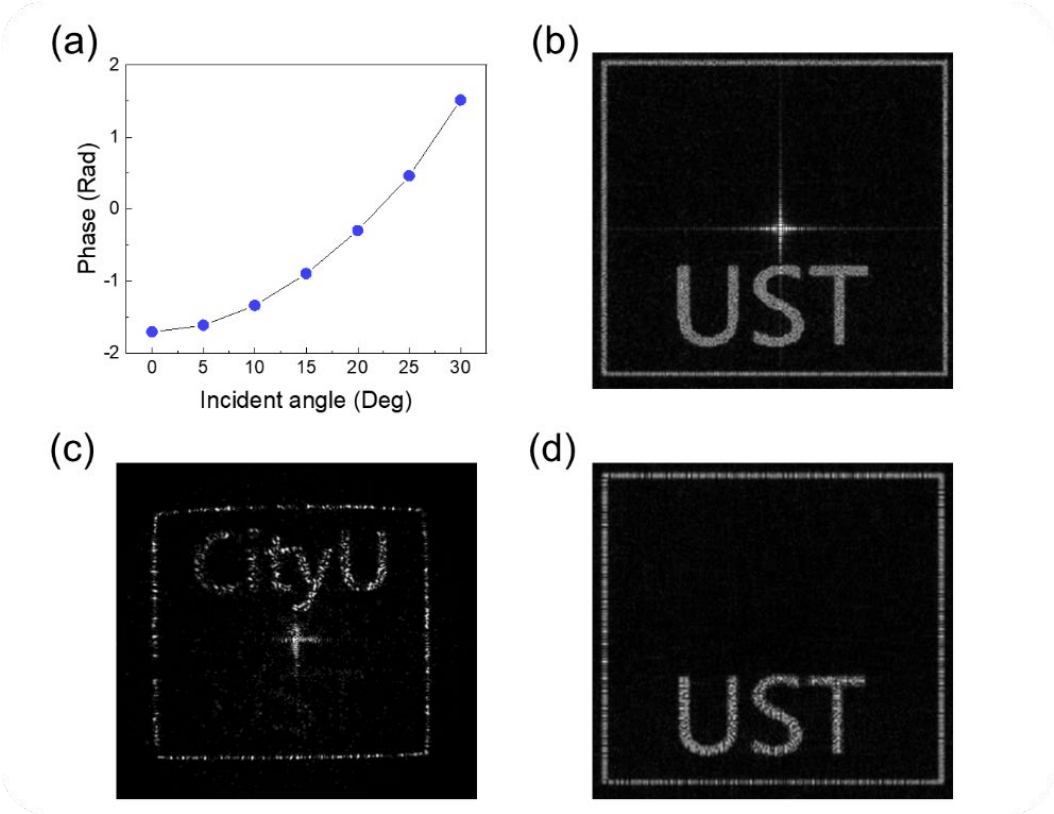

Figure S12 The explanation of the bright central spot and the executable solutions. (a) Modulation phase as a function of incident angle. (b) Far-field holographic calculation with 95% phase modulation efficiency. (c) Experimental results limiting incident angle and spot size. (d) Near-field holographic calculation with 95% phase modulation efficiency.